Scientific Research Publishing

Advances in Aerospace Science and Technology, 2025, 10(1), 18-33
https://www.scirp.org/journal/aast
ISSN Online: 2473-6724
ISSN Print: 2473-6708

The Study on the Aerodynamic Characteristics of the Transition Phase during the Take-Off of Compound Tilt-Wing Aircraft

Zhile Hong, Guoyi He, Xinxin Ouyang, Wentong Deng, Kaixu Zhang, Haitao Xu

Department of Aeronautics and Astronautics, Nanchang Hangkong University, Nanchang, China
Email: hegy509@163.com

How to cite this paper: Hong, Z.L., He, G.Y., Ouyang, X.X., Deng, W.T., Zhang, K.X. and Xu, H.T. (2025) The Study on the Aerodynamic Characteristics of the Transition Phase during the Take-Off of Compound Tilt-Wing Aircraft. *Advances in Aerospace Science and Technology*, **10**, 18-33.
https://doi.org/10.4236/aast.2025.101002

Received: February 26, 2025
Accepted: March 14, 2025
Published: March 17, 2025

Abstract

Compound tilt-wing aircraft have made innovations based on traditional tilt-rotor aircraft, offering advantages such as high efficiency, high speed, high stability, and high reliability. However, due to the uniqueness of their variable configurations, the aerodynamic characteristics during the tilt transition phase are extremely complex. This paper investigates the transition schemes and aerodynamic characteristics during the take-off transition phase by controlling boundary conditions such as flow velocity, lift rotor speed, pusher rotor pitch angle, and nonlinear speed transitions. The research results indicate that by controlling the uniform speed transition of boundary conditions, the total vertical force can overcome the aircraft's gravity to complete the transition from helicopter mode to fixed-wing mode. However, the total vertical force exhibits strong nonlinearity with changes in the tilt angle, which leads to the aircraft flying in a nonlinear climb posture during the take-off transition, resulting in poor safety and stability. After optimizing the nonlinear speed control of the boundary conditions, the total vertical force can change more stably with the tilt angle, allowing the aircraft to achieve a more stable altitude-hold transition flight, significantly improving the stability and safety of the flight.

Keywords

Compound Tilt-Wing, Momentum Source, Tilt Transition, Sliding Mesh

1. Introduction

In recent years, with continuous breakthroughs in aviation technology and the rapid rise of the low-altitude economy, electric Vertical Take-off and Landing (eVTOL) aircraft with vertical take-off and landing capabilities have become the focal point of global investors and research institutions [1]. These aircraft can

effectively alleviate urban traffic congestion and provide innovative solutions for the future urban air mobility (UAM) sector [2]-[4].

eVTOL aircraft come in a variety of models, primarily including multi-rotors, compound wing, and tilt-rotor configurations. These different configurations vary in terms of implementation complexity, flight speed, range, and application scenarios [5] [6]. The compound tilt-wing aircraft, as a derivative configuration of the tilt-rotor aircraft, is a new type of vertical take-off and landing vehicle that integrates the characteristics of tilt-rotor and compound wing, offering advantages in stability, safety, maneuverability, and efficiency. However, due to the special nature of the tilt-rotor aircraft's variant structure, during the tilt transition phase, where the aircraft switches between helicopter mode and fixed-wing mode, the aircraft's center of gravity continuously shifts. As a result, the aerodynamic loads exhibit highly nonlinear variations, making the control of such aircraft extremely challenging.

Globally, the aerodynamic characteristics of tilt-rotor aircraft and their derivative configurations during the tilt transition phase have become a hot topic in the field of aviation. Numerous scholars have conducted in-depth research on this complex aerodynamic issue. Currently, the research methods for aerodynamic characteristics during the tilt transition phase can be mainly categorized into experimental studies and numerical simulations. In terms of experimental research, scholars have used methods such as wind tunnel tests and flight testing to obtain key data, such as aerodynamic loads and flow field distribution, at different tilt angles [7]-[9]. On the numerical simulation side, with the rapid development of Computational Fluid Dynamics (CFD) technology, researchers have employed turbulence models like RANS and DES to simulate the complex flow field during the tilt process with high precision. These simulations have successfully modeled the interference phenomenon between the propeller slipstream and wing [10]-[12]. However, the existing research, both domestic and international, often focuses on simulating the tilt transition phase with fixed incoming flow speed, tilt angle, and blade pitch angle, which cannot effectively capture the continuity and unsteadiness of the transition phase. Additionally, most aerodynamic research on the tilt transition phase has focused on tiltrotor and tiltwing configurations, with limited studies on the aerodynamic characteristics of the tilt transition phase for compound tiltwing aircraft.

This paper uses CFD methods, combining the momentum source method with sliding mesh technology, to establish a numerical calculation approach that effectively simulates the continuous tilt transition phase of compound tiltwing aircraft. The study simulates the take-off transition phase of the compound tiltwing aircraft and analyzes the impact of different tilt strategies during the take-off tilt transition phase on the aerodynamic characteristics of the aircraft.

2. Numerical Simulation Method and Grid Model

2.1. Flow Control Equations and Momentum Source Method

In this study, the three-dimensional incompressible Reynolds-averaged Navier-

Stokes equations are used to describe and solve the tilt-transition phase of a compound tilt-rotor aircraft. Under the definition of the inertial coordinate system, the basic form of the three-dimensional incompressible Reynolds-averaged Navier-Stokes equation is:

$$\frac{\partial}{\partial t}\int_{v} \boldsymbol{W}\mathrm{d}v + \int_{\partial v} \left(\boldsymbol{F}_c - \boldsymbol{F}_v\right)\mathrm{d}s = \int_{v} \boldsymbol{S}\mathrm{d}v. \tag{1}$$

In Equation(1), $\boldsymbol{W}$ represents the variable for conservation of flow field, $\boldsymbol{F}_c$ represents the convection flux, $\boldsymbol{F}_v$ represents the viscous flux, $\boldsymbol{S}$ represents the source item, v represents the volume of the control body element, $\mathrm{d}v$ represents the surface of the control body element, $\mathrm{d}s$ represents the area of the control body element.

The momentum source method combines blade element theory with CFD calculations to obtain the local freestream velocities at the rotor blade sections. Based on the known geometric information of the section $\mathrm{d}F$, calculate the forces acting on this section. Then, incorporate these calculated forces into the momentum source terms $\mathrm{d}S$ for CFD simulations.

$$\mathrm{d}S = -N\mathrm{d}F\frac{\mathrm{d}\phi}{2\pi V_c}. \tag{2}$$

In Equation (2), N represents the number of impellers, $\mathrm{d}\phi$ represents the circumferential angle of a single blade, V_c represents the leaf element microelement volume. Then, obtain it through coordinate transformation $\mathrm{d}S_x$, $\mathrm{d}S_y$, $\mathrm{d}S_z$, and incorporate it into the momentum equation of the corresponding control volume grid cell for solving, iterating until convergence is achieved in the calculations.

2.2. Computational Model and Mesh Generation

To study the aerodynamic characteristics of the transition phase during the takeoff of a compound tilt-rotor aircraft, a preliminary geometric model of the aircraft has been established, as shown in Figure 1(a). This aircraft is a multi-propeller variant, designed with six propellers, four of which are lift rotors and two are pusher rotors. The lift rotors on the same side are mounted together on a cylindrical link connecting the wing and vertical tail. All rotors have identical design parameters, with each rotor equipped with five blades. The airfoil used is VR-5, the outer diameter of the rotor's radius is 1.45 m, and the hub radius is 0.27 m. Other detailed parameters of the aircraft are shown in Table 1. Since this study does not consider the impact of cross-sectional factors and aims to simplify the calculation, the interference from other components is neglected. Therefore, a half-model of one side of the aircraft, after removing the link, is used for simulation calculations.

During the CFD calculations, it is necessary to divide the flow field computational domain. In this study, the sliding mesh technique is used to simulate the tilt transition phase of the compound tilt-rotor aircraft. The flow field computational

domain of the sliding mesh requires the establishment of two flow regions. One is the dynamic domain (tilt domain), which includes the tilt-rotor section and the thrust propellers, while the other is the static domain, which includes the fixed-wing section, the front and rear lift propellers, and the fuselage. The final flow field computational domain is shown in **Figure 1(b)**, and it is a rectangular region with dimensions of 70 m × 70 m × 40 m, including a cylindrical tilt domain with a radius of 3.5 m and a height of 4m. The inlet is set as a velocity inlet, the outlet as a pressure outlet, the wing root plane as a symmetry plane, the wing surface as a wall, and the interface between the tilt domain and the outer domain is set as a sliding mesh interface. The remaining surfaces are set as sliding wall boundaries.

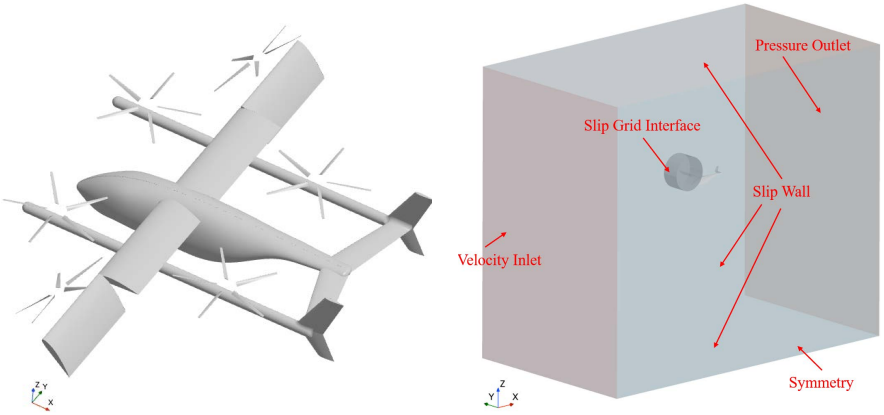

(a) Aircraft model (b) Computational domain model

Figure 1. Geometric model.

Table 1. Specific geometric parameters of compound tilting wing aircraft.

Parameter	Data	Parameter	Data
Wing airfoil	NACA4415	Blade airfoil	VR-5
Wingspan of a fixed-wing segment (m)	3.3	Rotor radius (m)	1.45
Wingspan of a tilt-wing segment (m)	3	Rotor root chord length (m)	0.141
Wing chord length (m)	1.125	Rotor tip chord length (m)	0.080
Rotor hub radius (m)	0.27	Number of blades	5

This study generates the computational mesh based on unstructured grid generation, which is mainly divided into two steps. First, the surface mesh of the computational model and the computational domain need to be generated, and then the volume mesh of the computational domain needs to be topologically filled. In the process of surface meshing, the maximum and minimum dimensions of the mesh are defined for the whole calculation model, and then some special surfaces are locally encrypted. When performing the volume meshing, to effectively simulate the boundary layer flow near the aircraft, a boundary layer mesh is generated on the aircraft surface, with the first layer mesh height set to 1.61209E − 5, the

number of prism layers set to 31, and the mesh growth rate set to 1.2. Then, similar to the generation of surface grids, the maximum and minimum dimensions of the overall domain volume grids are defined first, followed by local refinement of the volume grids. To ensure computational convergence, the dimensions of adjacent grids should not differ too much. Therefore, multiple grid refinement regions are established in the computational domain, with the grid dimensions gradually transitioning from fine to coarse from the inside to the outside. Additionally, since the power source method was used to replace the propeller in the aerodynamic characteristics study in this study, it was also necessary to carry out local volume mesh refinement of the virtual disk body at the location of the propeller, establish a cylinder with a radius of 1.5 m and a height of 0.2 m in the area where the blade was located, and carry out volume mesh refinement operations in this area. The final mesh division results in a total of 6.75 million mesh cells. Figure 2 shows the grid of the flow domain and the surface mesh of the aircraft.

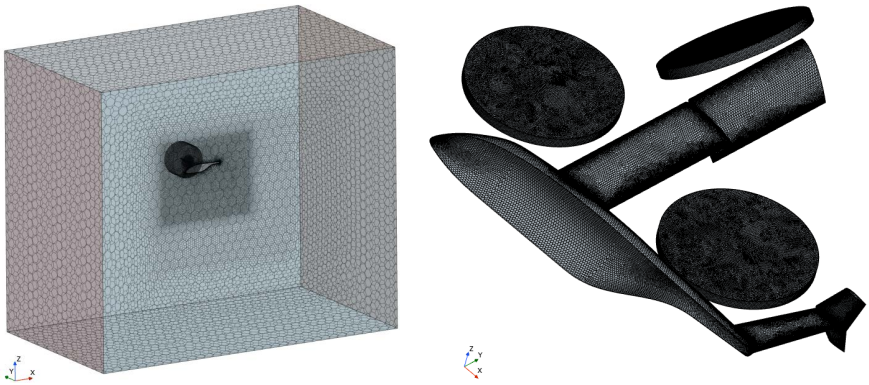

(a) Computational domain (b) Aircraft surface grid

Figure 2. Grid diagram of aircraft.

2.3. Grid Independence Verification

The quality and quantity of the grid have an important influence on the accuracy and efficiency of the calculation results. In order to ensure the reliability and efficiency of the calculation results, grid independence verification is carried out in this paper. The boundary conditions used for grid independence verification are as follows: flow velocity 80 m/s, fixed wing mode tilt Angle 0˚, Angle of attack 0˚, propeller speed 1000 RPM, and propeller pitch 0 deg. In the calculation process, the resolution of the grid is gradually improved. Starting from the rough grid, the number of grids gradually increases, and the grid is encrypted to check the changing trend of the calculation results. The calculation results are shown in Table 2. With the gradual encryption of the grid, the calculation results gradually become stable. After comparative analysis, considering the balance between the accuracy of the calculation results and the calculation efficiency, the grid with a number of 6.75 million was selected as the calculation grid in this paper. This grid quantity can not only ensure the accuracy of calculation, but also effectively control the time and resource

consumption required for calculation.

Table 2. Grid independence verification.

Number of grids (Millions)	Lift of aircraft (KN)	Drag of aircraft (KN)
537	10.125	0.870
675	10.168	0.864
759	10.162	0.865
982	10.163	0.863

3. Results and Analysis

In this study, based on the take-off weight of the aircraft, a systematic analysis was conducted on the different operating states of the aircraft in helicopter mode and fixed-wing mode. Specifically, the impact mechanisms of key parameters, such as the lift propeller rotational speed, flow velocity, and pusher rotor pitch, on the flight performance were explored.

3.1. Study on the Aerodynamic Characteristics of Uniform-Speed Tilt-Transition

3.1.1. Boundary condition

In helicopter mode, the aircraft primarily relies on the vertical lift generated by the lift rotors and thrust rotors to maintain flight, whereas, in fixed-wing mode, the aircraft achieves flight through the lift generated by the wings and the thrust provided by the pusher rotors, resulting in significant changes in its aerodynamic characteristics. In the take-off transition mode, by continuously transitioning from helicopter mode to fixed-wing mode at a uniform speed, the aerodynamic characteristics during the take-off transition process were studied and analyzed, providing a theoretical basis for achieving a smooth transition from helicopter mode to fixed-wing mode. The subject of this study is a compound tilt-wing aircraft with a take-off weight of 1900 kg and a cruising speed of 80 m/s in fixed-wing mode. To ensure that the vertical forces in both helicopter and fixed-wing modes before and after the take-off transition are sufficient to overcome gravity, flight conditions for both modes before and after the transition, as shown in Table 3, were set. Simulation results showed that the vertical forces in the two modes are 20.90 KN and 20.33 KN, respectively, both of which meet the requirements to overcome the aircraft's take-off weight.

To study the aerodynamic characteristics of the take-off transition segment and design a reasonable control scheme for the transition, a simulation of the unsteady boundary conditions with continuous uniform acceleration during the transition is conducted. In this simulation, the tilt time for the take-off transition segment is 5 seconds, with the lift rotor shutting down during the 4-second tilt of the wing segment. Parameters such as flight speed, lift rotor RPM, and propeller pitch change uniformly with time. The variation of each parameter with time is shown

in Figure 3.

Table 3. Flight conditions and total vertical forces in helicopter mode and fixed-wing mode.

Flight mode	Flow velocity (m/s)	Lift rotors speed (RPM)	Pusher rotor speed (RPM)	Pusher rotor pitch angle (DEG)	Total vertical force (KN)
Helicopter mode	8	1000	1000	0	20.90
Fixed-wing mode	80	0	1000	23	20.33

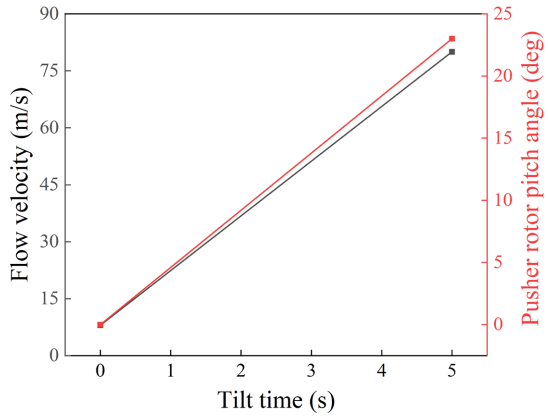

(a) Flow velocity and pusher rotor pitch angle

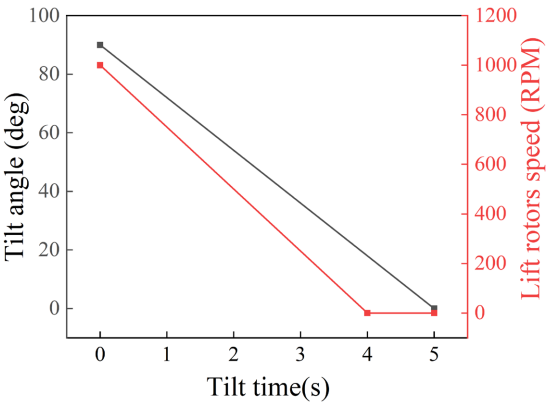

(b) Tilt angle and lift rotor speed

Figure 3. Take-off transition condition with uniform speed.

3.1.2. Calculation result

Figure 4 shows the vertical force variation with tilt angle for each component during the uniform acceleration transition. In the figure, L_f represents the fuselage lift, L_{in} represents the lift of the fixed-wing segment, L_{out} represents the lift of the tilt-wing segment, L_e represents the empennage lift, L represents the total lift of the aircraft, T_1 and T_2 represent the fore and aft lift rotor thrusts, T_{3z} represents the vertical component of the thrust rotor thrust, F_t represents the total of all vertical force components of the aircraft, G represents the weight of the aircraft, and

g is 9.8.

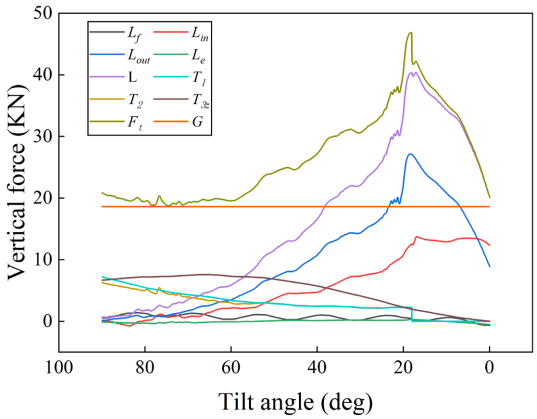

Figure 4. The vertical force of each component changes with the tilt angle.

As shown in **Figure 4**, as the tilt angle gradually decreases, the variation of F_t shows a trend of first increasing and then decreasing. Furthermore, F_t is always greater than the aircraft's weight, ensuring that the aircraft will not lose altitude due to a stall during the tilt transition segment. However, it is noteworthy that F_t is close to the weight of the aircraft during the initial stage of the take-off transition and in fixed-wing mode, but as the tilt angle decreases from 60˚ to 0˚, F_t is significantly higher than the weight, which causes the aircraft to experience a period of sustained climb during the take-off transition segment. This continuous upward trend leads to poorer stability and safety during flight. Analyzing the components of F_t, it is found that in the early stage of the take-off transition, F_t mainly comes from the thrust generated by the six sets of propellers. As the tilt angle decreases, the lift generated by the wings gradually increases and becomes the main contributor to F_t. T_1 and T_2 continuously decrease as the tilt angle decreases, and at a tilt angle of 18˚, the fore and aft lift rotors shut down and no longer generate thrust. Meanwhile, T_{3z} initially increases and then decreases as the tilt angle decreases, reaching zero at a tilt angle of 0˚.

According to the aerodynamic analysis of the aircraft itself, it can be found that L_f and L_e change gently with the decrease of tilt Angle, and their values are relatively small. On the other hand, the lift of the wing changes obviously, and L_{in} and L_{out} show different trends as the tilt Angle decreases. L_{in} continues to increase with the decrease of the tilting Angle, while L_{out} presents a trend of first increasing and then decreasing, in which the lift reaches the maximum when the tilting Angle is 18˚. The growth rate of L_{in} is much smaller than that of L_{out}, and the tilting wing segment has stronger dynamic change characteristics in the generation of lift force.

Figure 5 shows the curve of the total lift coefficient (C_L) of the variable-geometry transition aircraft varying with the tilt angle. As can be seen from the figure, due to the nonlinear and unsteady aerodynamic characteristics of the tilt transition section of the compound tilt wing, C_L exhibits relatively significant fluctuations

around the tilt angle of 80˚. As the tilt angle gradually decreases, C_L continues to decline. C_L drops sharply during the tilt angles from 90˚ to 70˚ and from 20˚ to 0˚, while it remains relatively stable between 70˚ and 20˚. This trend is significantly different from the variation law of L with the tilt angle. The difference mainly originates from the changes in the incoming flow velocity and the reference area of the tilt-wing section during the take-off transition process of the aircraft.

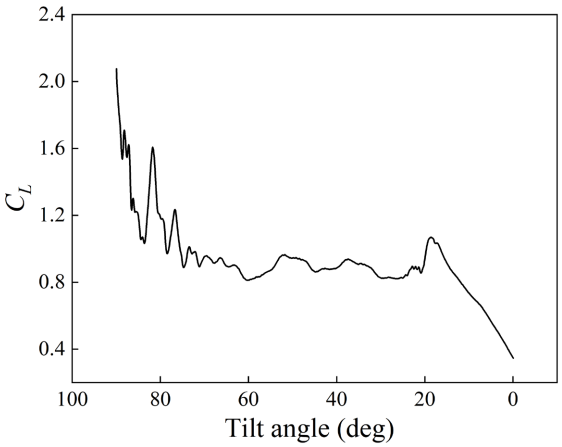

Figure 5. The total lift coefficient of the aircraft varies with the tilt angle.

3.1.3. Result Analysis

Figure 6(a) and **Figure 6(b)** show the velocity contour plots of the x-z cross-section through the centers of the lift and propulsive rotors, as well as the pressure coefficient contour plots on the fuselage surface, viewed from the front and rear axes, under different tilt angles during the variable-speed transition phase. From the figures, it can be observed that in the early stage of the take-off transition phase, the slipstream effect of the rotors is significant, with the rotors providing the primary vertical force for the aircraft. As the tilt angle decreases, the rotational speed of the lift rotor reduces, leading to a diminished slipstream effect and a corresponding decrease in the thrust generated by the lift rotor. In contrast, the slipstream effect of the propulsive rotor remains pronounced throughout the transition phase. However, due to the change in direction, its vertical force also decreases accordingly. At a tilt angle of 90˚, the slipstream of the propulsive rotor can effectively adhere to the upper surface of the tilting wing segment. However, at tilt angles of 72˚, 54˚, and 36˚, as the incoming flow velocity increases, the slipstream from the propulsive rotor exhibits significant flow separation on the upper surface of the tilting wing segment, with the most pronounced separation occurring at a tilt angle of 36˚. After the tilt angle reaches 18˚, the flow separation on the upper surface of the tilting wing segment disappears due to the change in the direction of the slipstream from the propulsive rotor. Since the tilt angle of approximately 18˚ is the critical angle for flow separation on the upper surface of the tilting wing, the lift generated by the tilting wing reaches its maximum value at this angle.

Regarding the pressure coefficient distribution on the aircraft surface, at a tilt angle of 90˚, the upper surface of the aircraft exhibits a relatively large negative pressure region. This is attributed to the influence of the slipstream from the lift rotor, which induces a significant negative pressure area on the upper fuselage surface. Compared to the 90˚ tilt angle, the negative pressure region on the upper surface of the aircraft is relatively reduced between tilt angles of 72˚ and 36˚. However, the pressure difference remains relatively stable within this range of tilt angles. At tilt angles of 18˚ and 0˚, the negative pressure region on the upper surface of the aircraft initially increases and then decreases. The changes in the surface pressure coefficient during the take-off transition phase, along with variations in the incoming flow velocity and the reference area of the tilting wing, directly lead to the alterations in the lift and lift coefficient of the aircraft.

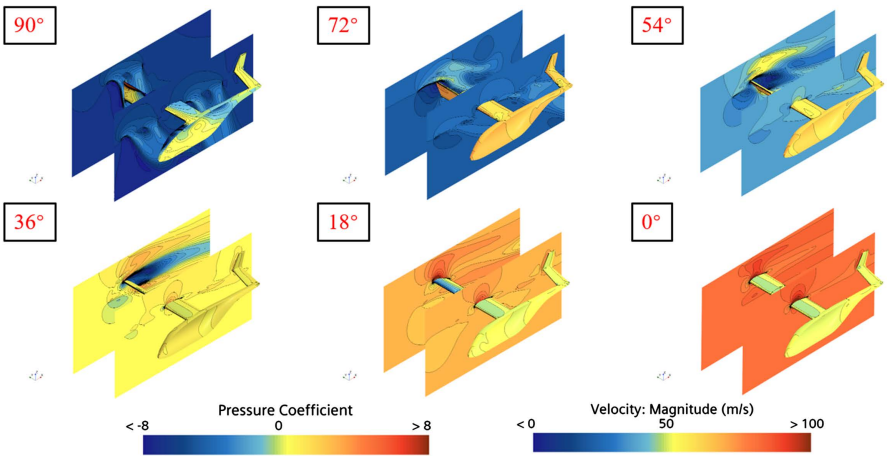

(a) Front axle view

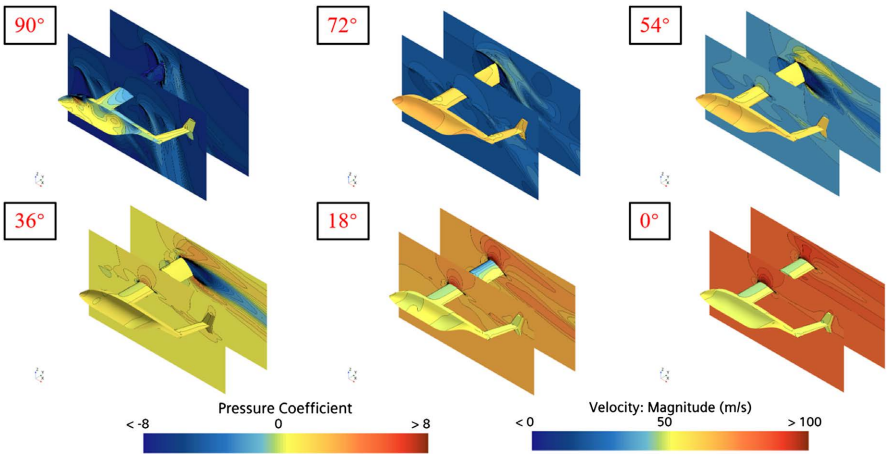

(b) Rear axle view

Figure 6. Velocity cloud image of different tilt angle sections and surface pressure coefficient cloud image of aircraft.

The transition of the aircraft from helicopter mode to fixed-wing mode is achieved through uniformly accelerated control of the boundary conditions. During the entire transition phase, the aircraft exhibits a nonlinear climbing attitude. This climbing

state implies that the aircraft is unable to achieve an ideal stable flight condition. Although this transition method can sustain flight to some extent, it is not the optimal flight state and fails to fully exploit the aerodynamic performance and lift characteristics of the compound tilt-wing aircraft.

3.2. Study on Aerodynamic Characteristics of Nonlinear Variable Speed Tilting Transition

3.2.1. Boundary Condition

To achieve stable flight at a constant altitude during the take-off transition phase, further optimization of the boundary condition transition scheme is required. Considering that in the early stage of the transition, the vertical force of the aircraft primarily originates from the pusher rotors, while in the later stage, it mainly relies on the lift generated by the wings, the flow velocity of the aircraft is relatively reduced during the initial tilt phase and then increased in the later stage of the transition. For the lift rotor rotational speed, the deceleration process in the early stage of the transition should be slowed down, while the deceleration process should be accelerated in the later stage. Additionally, as observed in the previous section, the vertical thrust of the propulsive rotor first increases and then decreases. Therefore, pitch control of the propulsive rotor is suspended in the early stage of the tilt transition and gradually reintroduced with increasing pitch acceleration in the later stage. The tilt angle is maintained at a uniform rate of change, and the specific nonlinear variable-speed transition conditions are shown in Figure 7.

3.2.2. Calculation Result

Figure 8 presents the curves of the vertical forces of each component as a function of the tilt angle during the nonlinear variable-speed transition. From the figure, it can be observed that after optimizing the take-off transition conditions, the total vertical force F_t is slightly greater than the gravitational force and remains relatively stable throughout the take-off transition phase. This indicates that a relatively stable constant-altitude flight can be achieved during the entire take-off transition phase, with high stability and safety of the flight.

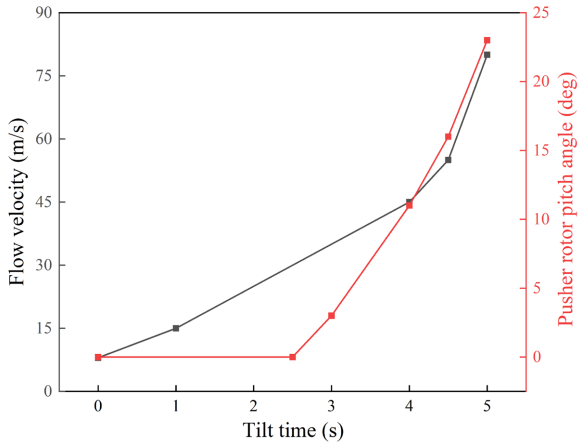

(a) Flow velocity and pusher rotor pitch angle

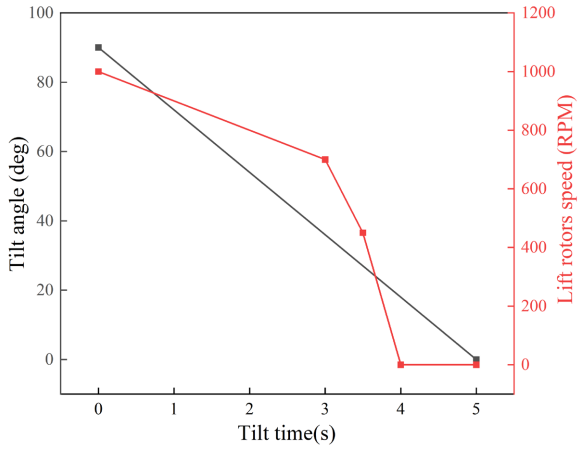

(b) Tilt angle and lift rotor speed

Figure 7. Take-off transition condition with uniform speed.

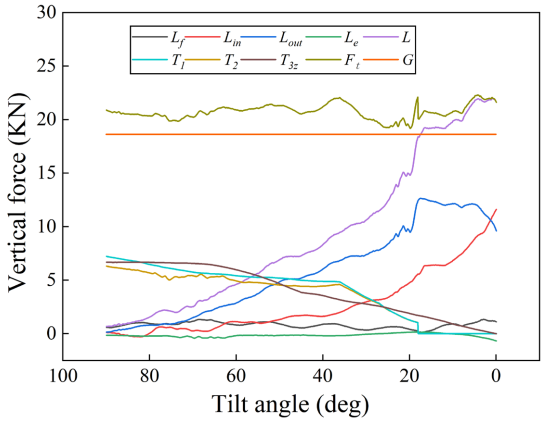

Figure 8. The vertical force of each component changes with the tilt angle.

Analyzing the composition of F_t in detail, it is similar to the uniformly accelerated transition case. In the early stage of the transition, F_t is mainly provided by the vertical thrust of the rotors. In the later stage of the transition, the vertical thrust of the rotors decreases, and the aerodynamic force of the aircraft gradually increases, becoming the main component of F_t in the later stage. By optimizing the transition methods of the lift rotor speed and the propulsive rotor pitch, T_1 and T_2 decrease at a slower rate in the early stage of the tilt transition phase and then drop to zero at a faster rate in the middle and late stages, matching the growth rate of the wing lift, so that the total vertical force does not deviate too much from the gravitational force. At the same time, the variation trend of T_{3Z} is similar to that of the lift rotor, showing a nearly uniformly accelerated linear decrease process.

In the analysis of the aerodynamic forces of the aircraft itself, the trend and overall magnitude of L after a tilt angle of 18˚ exhibit significant differences compared to the uniformly accelerated transition mode. L continuously increases with the reduction of the tilt angle and reaches its maximum value at a tilt angle of 0˚. In contrast, L_f and L_e behave similarly to the uniformly accelerated transition mode, with smaller

magnitudes and relatively stable variations that are less affected by changes in the tilt angle. The variation in L is primarily attributed to the lift generated by the wings. The trends of L_{in} and L_{out} during the reduction of the tilt angle are almost entirely consistent with those observed in the uniformly accelerated transition mode before a tilt angle of 18˚. However, once the tilt angle exceeds 18˚, a significant change occurs. At this point, the lift generated by the fixed-wing segment increases sharply, while the lift from the tilting-wing segment initially decreases at a relatively gentle rate before rapidly declining. These distinct trends in lift variation, especially after a tilt angle of 18˚, are the key factors leading to the different trends in L under the two take-off transition modes. Under the nonlinear variable-speed transition mode, the rapid increase in incoming flow velocity after a tilt angle of 18˚ results in more intense and uneven changes in lift. Due to the differences in the distribution of incoming flow velocity between the uniformly accelerated and nonlinear transitions, although the overall trends in lift variation with tilt angle appear similar at certain angles, the lift magnitude in the uniformly accelerated transition mode is greater.

Figure 9 presents the polyline chart of the total lift coefficient of the nonlinear variable-speed transition aircraft as a function of the tilt angle. Similar to the uniformly accelerated transition, there are also relatively significant fluctuations near the tilt angle of 80˚. Overall, the lift coefficient exhibits a continuous downward trend. Compared with the uniformly accelerated transition mode, the rate of decline is relatively stable, with the lift coefficient gradually decreasing without the abrupt downward trend observed in the uniformly accelerated transition mode. Under this mode, the aircraft is better able to maintain a more stable lift characteristic.

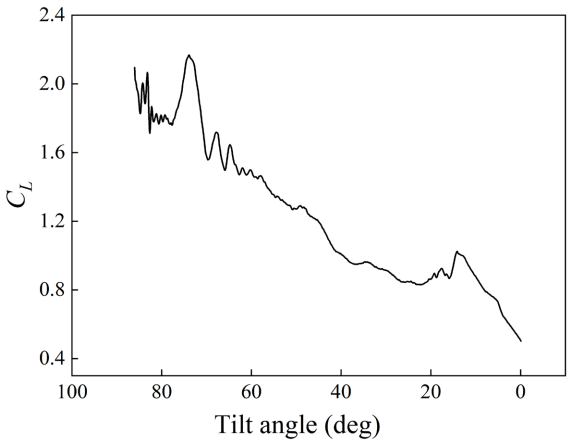

Figure 9. The total lift coefficient of the nonlinear variable speed transition vehicle varies with the tilt angle.

3.2.3. Result Analysis

Figure 10(a) and Figure 10(b) show the velocity contour plots of the x-z cross-section through the centers of the lift and propulsive rotors, as well as the pressure coefficient contour plots on the fuselage surface, viewed from the front and rear axes, under different tilt angles during the nonlinear variable-speed transition. Comparing these contour plots with those of the uniformly accelerated transition,

it is found that after optimizing the transition state, the rate of attenuation of the lift rotor slipstream is reduced. At a tilt angle of 54˚, a strong slipstream from the lift rotor is still visible. Correspondingly, in the early stage of the take-off transition, T_1 and T_2 do not decrease at an excessively rapid rate, thereby ensuring the stability of flight. Although the propulsive rotor slipstream exhibits a stall characteristic on the upper surface of the tilting wing segment similar to that observed during the uniformly accelerated transition, the slipstream effect of the propulsive rotor is weaker in the early stage of the tilt transition, and the incoming flow velocity is relatively low, resulting in a relatively weaker stall characteristic. Although the tilting wing segment is still in the critical region of flow separation at a tilt angle of 18˚, the incoming flow velocity increases rapidly after this angle, preventing a rapid decrease in lift on the tilting wing segment after 18˚. Regarding the distribution of the aircraft surface pressure coefficient, the variation trend is the same for both nonlinear variable-speed and uniformly accelerated transitions. However, due to the different velocity variation trends of the two transition modes, the lift and lift coefficient are different.

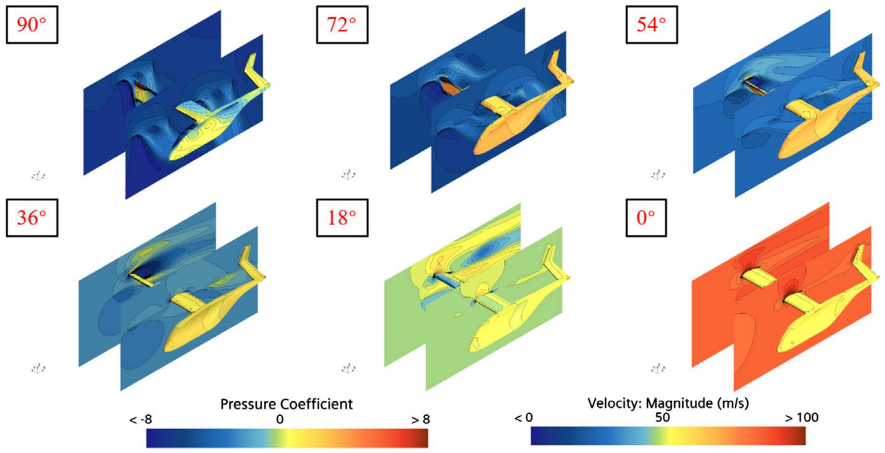

(a) Front axle view

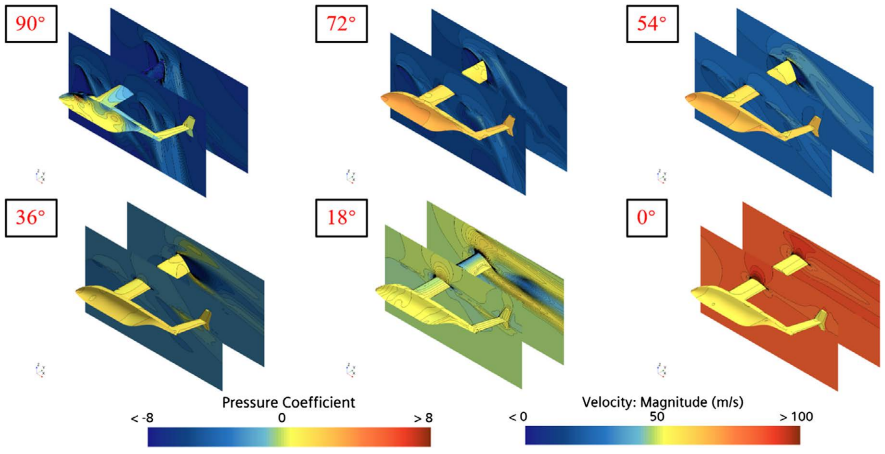

(b) Rear axle view

Figure 10. Velocity cloud image of different tilt angle sections and surface pressure coefficient cloud image of aircraft.

Through simulation and analysis of the nonlinear variable-speed transition during the take-off phase of the compound tilt-wing aircraft, it is evident that stable constant-altitude transition flight can be achieved by controlling the boundary conditions during the take-off transition. However, a detailed examination of the lift coefficient and contour plots reveals that, despite the total vertical force of the aircraft maintaining a relatively stable value with changes in the tilt angle, the aerodynamic coefficients and contour plots still exhibit highly nonlinear and unsteady characteristics.

4. Conclusions

In this paper, the take-off transition phase of the compound tilt-wing aircraft is simulated and analyzed through both uniformly accelerated and nonlinear variable-speed transition controls, which involve regulating the incoming flow velocity, lift rotor rotational speed and propulsive rotor pitch. After comparing the computational results, the following conclusions are drawn:

- Although the aircraft can overcome gravity and complete the take-off transition from helicopter mode to fixed-wing mode through uniformly accelerated transition, the total vertical force F_t exhibits nonlinear variation with the change in tilt angle during the transition. This leads to a nonlinear climbing attitude during the take-off transition, resulting in poor stability and safety. Moreover, the lift and lift coefficient of the aircraft show strong nonlinearity with the change in tilt angle, and the velocity and pressure coefficient contour plots reveal highly unsteady characteristics.
- By implementing a nonlinear variable-speed transition for the boundary conditions during the take-off transition of the compound tilt-wing aircraft, the total vertical force F_t changes more stably with the tilt angle, allowing the aircraft to achieve a more stable constant-altitude transition flight, significantly enhancing the stability and safety of the flight. However, a detailed analysis of the aerodynamic forces and coefficients still reveals that the take-off transition of the compound tilt-wing aircraft possesses very complex aerodynamic characteristics.

Funding

National Natural Science Foundation of China: The hydrodynamic mechanism of stable formation in self-propelled fish schools (Fund Number: 12362026).

Conflicts of Interest

The authors declare no conflicts of interest regarding the publication of this paper.

References

[1] Liu, K. and Ye, F.C. (2015) Review and Analysis of Recent Developments for VTOL Vehicles. *Advances in Aeronautical Science and Engineering*, **6**, 127-138.

[2] Coppola, P., De Fabiis, F. and Silvestri, F. (2024) Urban Air Mobility (UAM): Airport Shuttles or City-Taxis? *Transport Policy*, **150**, 24-34. https://doi.org/10.1016/j.tranpol.2024.03.003

[3] Straubinger, A., Rothfeld, R., Shamiyeh, M., Büchter, K., Kaiser, J. and Plötner, K.O. (2020) An Overview of Current Research and Developments in Urban Air Mobility—Setting the Scene for UAM Introduction. *Journal of Air Transport Management*, **87**, Article ID: 101852. https://doi.org/10.1016/j.jairtraman.2020.101852

[4] Spühler, F., Siebenrock, K., Terekhov, I. and Mattfeld, D.C. (2025) A Framework for Ranking Potential Cities for Implementing Emerging Urban Mobility Technologies: A Case Study for eVTOL Aircraft. *Journal of Urban Mobility*, **7**, Article ID: 100102. https://doi.org/10.1016/j.urbmob.2025.100102

[5] Bacchini, A. and Cestino, E. (2019) Electric VTOL Configurations Comparison. *Aerospace*, **6**, Article No. 26. https://doi.org/10.3390/aerospace6030026

[6] Deng, J.H. (2024) Key Technologies and Development for High-Speed Helicopters. *Acta Aeronautica et Astronautica Sinica*, **45**, 47-69.

[7] Johnson, W., Yamauchi, G., Derby, M. and Wadcock, A. (2003) Wind Tunnel Measurements and Calculations of Aerodynamic Interactions between Tiltrotor Aircraft. 41*st Aerospace Sciences Meeting and Exhibit*, Reno, 6-9 January 2003, 47. https://doi.org/10.2514/6.2003-47

[8] Zanotti, A., Velo, A., Pepe, C., Savino, A., Grassi, D. and Riccobene, L. (2024) Aerodynamic Interaction between Tandem Propellers in eVTOL Transition Flight Configurations. *Aerospace Science and Technology*, **147**, Article ID: 109017. https://doi.org/10.1016/j.ast.2024.109017

[9] Droandi, G., Gibertini, G., Grassi, D., Campanardi, G. and Liprino, C. (2016) Proprotor-Wing Aerodynamic Interaction in the First Stages of Conversion from Helicopter to Aeroplane Mode. *Aerospace Science and Technology*, **58**, 116-133. https://doi.org/10.1016/j.ast.2016.08.013

[10] Li, P. and Zhao, Q.J. (2016) CFD Analyses of Aerodynamic Characteristics of Tiltrotor under Typical Flight Conditions. *Journal of Aerospace Power*, **31**, 421-431.

[11] Poling, D.R., Rosenstein, H. and Rajagopalan, G. (1998) Use of a Navier-Stokes Code in Understanding Tiltrotor Flowfields in Hover. *Journal of the American Helicopter Society*, **43**, 103-109. https://doi.org/10.4050/jahs.43.103

[12] Wang, Y.C. He, G.Y. and Wang, Q. (2022) Aerodynamic Performance Analysis and Optimization of Tilt-Wing UAV in Return Transition Section. *Science Technology and Engineering*, **22**, 9848-9856.